

Magnetic and Optical Study of Zinc Ferrite Produced by the Ceramic Method



Mery C. Gómez-Marroquín, Fernando Huamán-Pérez, Henry Colorado, Nilton Cárdenas-Falcón, José Carlos D'Abreu, Abraham J. Terrones-Ramirez, and Kim J. Phatti-Satto

Abstract A solid–solid reaction took place at 1000 °C during 4 h, using a mixture of pure iron oxide Fe_2O_3 and pure zinc oxide— ZnO in order to synthesize zinc ferrite—ZF of different compositions: (S1) $\text{Fe}_2\text{O}_3/\text{ZnO}:3/2$, (S2) $\text{Fe}_2\text{O}_3/\text{ZnO}:1/1$, (S3) $\text{Fe}_2\text{O}_3/\text{ZnO}:4/1$, and (S4) $\text{Fe}_2\text{O}_3/\text{ZnO}:2/1$. Each of these mixtures were milled during 24 h before the thermic treatment was carried out. S1, S2, S3, and S4 samples were become to M1, M2, M3, and M4 samples, respectively, which after that were thermally characterized using DSC, DTA, and TG techniques. In sequence the ZF produced were examined using XRD, optical, and magnetic techniques, SEM and TEM. XRD analysis shows up contains of equimolar ZF: M3 (73.20%), M4 (28.00%), and M2 (2.10%) as non-stoichiometric phases of ZF: 31.80% of $\text{Zn}_{0.95}\text{Fe}_{1.78}\text{O}_{3.71}$ and 30.40% of $\text{Zn}_{1.08}\text{Fe}_{1.92}\text{O}_4$ in M4; $\text{Zn}_{0.97}\text{Fe}_{2.02}\text{O}_4$ in M3 and 35.30% of $\text{Zn}_{0.54}\text{Fe}_{2.46}\text{O}_4$ in M1. Previous studies of magnetic characterization observed a little hysteresis of

M. C. Gómez-Marroquín (✉) · F. Huamán-Pérez · A. J. Terrones-Ramirez · K. J. Phatti-Satto
Steelmaking and Ironmaking Research Group, National University of Engineering, 210 Túpac Amaru Ave, Rímac, Lima 15333, Peru
e-mail: mgomez@uni.edu.pe

F. Huamán-Pérez
e-mail: fhuaman@uni.edu.pe

A. J. Terrones-Ramirez
e-mail: abraham.terrones@uni.pe

K. J. Phatti-Satto
e-mail: kphattiss@uni.pe

H. Colorado
University of Antioquia, 67 St, 52-21, 1226 Medellín, Antioquia, Colombia
e-mail: henry.colorado@udea.edu.co

N. Cárdenas-Falcón
Pontifical Catholic University of Perú, Universitaria Ave, 1801, San Miguel, Lima 15088, Peru
e-mail: ncardenasf@pucp.edu.pe

J. C. D'Abreu
Pontifical Catholic University of Rio de Janeiro, Marquês de São Vicente St, 225 Gávea, Rio de Janeiro, RJ 22522451-900, Brazil
e-mail: dabreu@puc-rio.br

this equimolar ZF. The results of estimation of the bandgap energy (E_g) via the manipulation of the Kubelka–Munk theory allowed to determine that the samples M1, M2, M3, and M4 are considered semiconductors (3.66 and 3.76 eV).

Keywords Ceramic method · Magnetic materials · Zinc ferrite—ZF · Optical characterization · Magnetic characterization · Modified Kubelka–Munk function

Introduction

As is known, zinc ferrite is a spinelium compound that belongs to the franklinite family. Spinelias are constituted as a group of minerals that crystallize in the cubic system, with an octahedral habit. Its general formula is $(X)(Y)_2O_4$, where X represents the cations that occupy tetrahedral positions and Y the octahedral ones. Some divalent, trivalent and tetravalent cations can occupy the X and Y positions, including elements such as: Mg, Zn, Fe, Al, Cr, Ti, and Si [1]. Zinc ferrites can be normal (when Zn atoms occupy tetrahedral sites and Fe atoms occupy octahedral sites) or inverse (when Zn atoms partially occupy the octahedral sites, while Fe atoms occupy half of the octahedral sites) [2, 3]. There are different methods for synthesizing zinc ferrites, including conventional ceramic, mechanochemical, sol–gel synthesis, combustion technique, hydrothermal processing, etc. [3, 4], but the ceramic route has allowed the formation of either stoichiometric or equimolar zinc ferrites, defined mainly at high synthesis times and temperatures, 4 h and 1000 °C, respectively [5]. These materials are considered ferromagnetic, and due to their good magnetic and optical properties, they can be used in electronic applications mainly, magnetic recording and fluids, catalysis, sensors, magnetically guided drug delivery, pigments, microwave technology, catalytic and biomedical fields [6]. On the other hand, optical analysis (UV-Vis and PL) of zinc ferrites nanoparticles had been studied demonstrating their absorption edge properties in the visible region which is legitimated to the excitation of electron from O-2p state to Fe-3d state [7]. Various zinc ferrite characterization techniques were used to determine the crystallinity, crystallite size, lattice parameter, morphology, elemental composition, energy bandgap, emission, saturated magnetization, and coercivity of the synthesized nanoparticles [8]. This work is aimed to understand the relationship between the magnetic and optical study of zinc ferrite samples produced by the ceramic method but using non-stoichiometric and stoichiometric mixtures [9].

Table 1 Molar and weight ratios of raw materials for preparation of stoichiometric and non-stoichiometric mixtures

Samples	Molar ratio		Weight ratio		Heat treatment product names
	Fe ₂ O ₃	ZnO	Fe ₂ O ₃	ZnO	
S1	3	2	3.23	1	M1, M'1
S2	1	1	2.16	1	M2, M'2
S3	4	1	8.63	1	M3, M'3
S4	2	1	4.32	1	M4, M'4
ZF pure	1	1	2.00	1	M5
Hematite	1	–	1.00	–	HM

Experimental Procedures

Mechanical Preparation of Stoichiometric and Non-stoichiometric Mixtures

The raw materials, zinc oxide and iron(III) oxide, were prepared mechanically through simultaneous grinding and homogenization using 500 g ceramic mortars and 25 g agate mortars, simulating grinding in a ball mill.

Thermogravimetric Analysis via DTG and TGA

For this purpose, a Perkin Elmer TGA 4000 analyzer with S/N: 522A17110904 was used. For this reason, we proceeded to take approximately 10 mg by weight of each of the stoichiometric oxide mixtures: Fe₂O₃/ZnO:1/1 (S2) and non-stoichiometric Fe₂O₃/ZnO:3/2 (S1), Fe₂O₃/ZnO:4/1 (S3), and Fe₂O₃/ZnO:2/1 (S4) previously homogenized and ground in mortars (Table 1).

This test took place via programming a heating ramp of the thermogravimetric analysis equipment under the following operating conditions: Heating rate of 10 °C/min, initial temperature of 30 °C to final temperature of 900 °C, isothermal period 5 min at 900 °C, and inert gas flow (N₂) of 50 mL/min.

Heat Treatment of Oxide Mixtures

Samples of 100–150 g of stoichiometric mixtures were then weighed: Fe₂O₃/ZnO:1/1 (S2) and non-stoichiometric mixtures: Fe₂O₃/ZnO:3/2 (S1), Fe₂O₃/ZnO:4/1 (S3), and Fe₂O₃/ZnO:2/1 (S4) which were weighed, homogenized, and ground for 24 and 48 h. Four porcelain crucibles with a maximum capacity of 125 g were preheated



Fig. 1 Mechanical preparation and mortar grinding of raw materials and heat treatment or synthesis of zinc ferrites followed by their mechanical preparation for complete characterization

at a temperature of 300 °C for a period of 8–12 h, before subjecting them to a heat treatment at 1000 °C for 4 h, together with the 4 prepared mixes. These thermal treatments were carried out in a FUNDINORT S.A.C brand electric muffle furnace of 1100 °C maximum temperature previously calibrated and which showed a heating rate of approximately 1.5 °C/min. The samples weighed in the proportions S1, S2, S3, and S4, which were ground and mixed for about 24 h, became M1, M2, M3, and M4, and those of 48 h became M'1, M'2, M'3, and M'4; after heat treatment.

The molar and weight proportions of these mixtures, as well as the names of the products obtained after heat treatment, are presented in Table 1.

The samples called thermal treatment products (M1, M2, M3, M4, and M5) were used to carry out the structural characterization, via XRD, magnetic-VSM, and optical-UV vis. Figure 1 shows the mechanical mixing and grinding of the raw materials carried out in ceramic mortars, before heat treatment, and the heat treatment or synthesis of zinc ferrites followed by their mechanical preparation for their complete characterization of the samples. Only samples M'1, M'2, M'3, and M'4 were analyzed by XRD.

X-Ray Diffraction Analysis—XRD

XRD of raw materials (mixtures treated thermally) was performed in an ADVANCE D8 X-ray diffractometer, BRUKER. This equipment is scanned with a goniometer (radius 240 mm). XRD patterns were collected in the 2θ range of 5°–90° with 0.02° increment and a divergence slit size of 0.6°. The diffractometer has copper anodes ($\lambda = 1.5406 \text{ \AA}$, Cu K- α ; $\lambda = 1.39225 \text{ \AA}$, Cu K- β), and operates with a 40 kV voltage and a 30 mA current. We analyze the crystalline phases and/or inorganic compounds in the tested samples qualitatively (by comparison with the ICSD database) and quantitatively (using the Rietveld method).

Magnetic Characterization—VSM

These tests for determination of magnetic properties were carried out in a Vibrating Sample Magnetometer (VSM) brand GLOBALMAG and model TMAG-V2, which has a Gaussian magnetic field of $1 \text{ T/V} \approx 10 \text{ Oe/mV}$ sensitivity and passage speed of 16.8 Oe/s . This equipment operated with a Stanford Research System Locking Amplifier, Model SR830 with a generator configuration of $[-8 \text{ A}, 8 \text{ A}]$ and $[-50 \text{ V}, 50 \text{ V}]$.

Optical Characterization—UV Vis

The optical characterization was carried out using a Shimadzu UV-2600 spectrophotometer (A11665704761) coupled to UVProbe software version 2.7 that measured absorbance and reflectance in a wavelength range of $300\text{--}700 \text{ nm}$, average scanning speed, interval of sampling of 0.05 nm , absorbance and reflectance slit width of 5.0 nm , accumulation time of 2.0 s , light source switching wavelength: 370.0 nm detector unit: external (2 detectors) detector wavelength switching: 900.0 nm S/R exchange.

Results and Discussion

TGA-DTG Thermogravimetric Analysis

Figure 2a shows the TGA thermogram of the weight loss tests of the samples: S1, S2, S3, and S4 while Fig. 2b shows the behavior of the samples S1, S2, S3, and S4 against to the heating time and temperature in the thermogravimetric equipment, where St1, St2, St3, and St4 are the programmed temperatures and ST1, ST2, ST3, and ST4 are the temperatures observed by the corresponding samples S1, S2, S3, and S4.

As expected, all treated samples showed a weight loss during treatment at $1000 \text{ }^\circ\text{C}$ for 4 h due to the evaporation of zinc that was part of its corresponding oxide. Knowing that both samples S2 and S3 showed both the minimum and maximum weight loss of the four samples tested, respectively. However, the DTA-DTG test of the four samples showed that all of these lost almost the same weight from the temperature of the environment to approximately $100 \text{ }^\circ\text{C}$, possibly due to the humidity gained during its preparation and grinding. Sample S4 showed a very close weight loss compared to sample S3. The stoichiometric sample, S2 showed a weight loss of approximately 0.02% . Because the weight losses of the tested samples are negligible, it can be considered that they are stable against heat treatment at high temperatures.

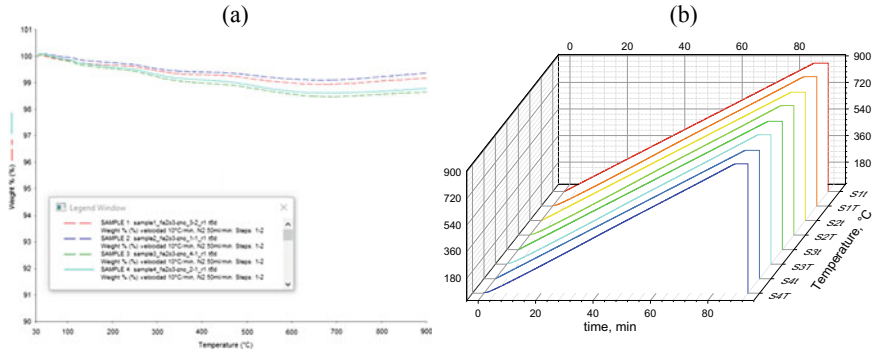


Fig. 2 a Weight loss thermogram of samples S1, S2, S3, and S4, and b 3D behavior of samples S1, S2, S3, and S4 versus heating time and temperature in the thermogravimetric equipment

See Fig. 3. Next, Table 3 shows the weight losses of the DTA-DTG assay and the main endothermic peaks of the samples: S1, S2, S3, and S4.

Using the main endothermic peaks obtained during the TGA-DTG test of the samples: S1, S2, S3, and S4, and the quantification of crystalline phases carried out by the XRD analysis, the formation of the main spinels of the zinc ferrites can be verified, both stoichiometric and non-stoichiometric (mixed). It has also been observed that both samples S1 and S2 showed a very insignificant weight loss between 0.02 and 0.25% and samples S3 and S4 a significant weight loss between 1.00 and 1.10%.

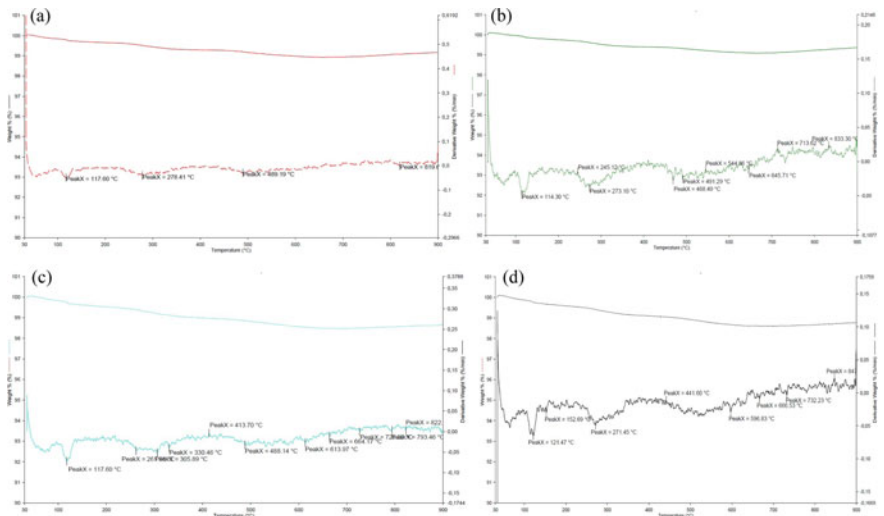


Fig. 3 TGA and DTG curves of the decomposition of the sample a S1 ($T = 117.6$ °C), b S2 ($T = 114.3$ °C), c S3 ($T = 117.60$ °C), and d S4 ($T = 121.4$ °C)

Table 3 Weight losses of the DTA-DTG test and the main endothermic peaks of the samples: S1, S2, S3, and S4

Samples	% Weight loss—TGA	Endothermic peaks of probable appearance of the spinel phase of zinc ferrite—DTG (°C)
S1	0.05	117.60, 278.41, 489.19, and 819.60
S2	0.02	114.30, 273.10, 468.49, 491.29, 544.86, 645.71, 713.62, and 833.30
S3	1.10	117.60, 261.08, 305.89, 330.46, 413.70, 488.14, 613.97, 664.17, 728.80, 793.46, and 822.30
S4	1.00	121.47, 271.45, 441.60, 596.83, 666.53, 732.23, and 847.00

Likewise, samples S1 and S3 show in common a first and only endothermic peak or coincident decomposition temperature equal to 117.60 °C.

Characterization via X-Ray Diffraction-XRD

Figure 4 shows (a) the diffractogram of the XRD analysis of M4, and (b) the diffraction patterns of samples M1, M2, M3, and M4, as well as, Tables 4 and 5 the main crystalline phases identified and quantified by the Rietveld method of the XRD of the samples: M1, M2, M3, and M4, as well as, the samples M'1, M'2, M'3, and M'4, respectively.

Certainly, the spinel phases present in both Tables 4 and 5 obey the formula: $[A_{1-x}B_x]t[A_xB_{1-x}B]oO_4$. As can be seen, the four samples tested after 24 h of grinding: M1, M2, M3, and M4 show the presence of the main inverse spinel phases both in the stoichiometric form: $ZnFe_2O_4$ in M3 (73.20%), M4 (28.00%), and M2

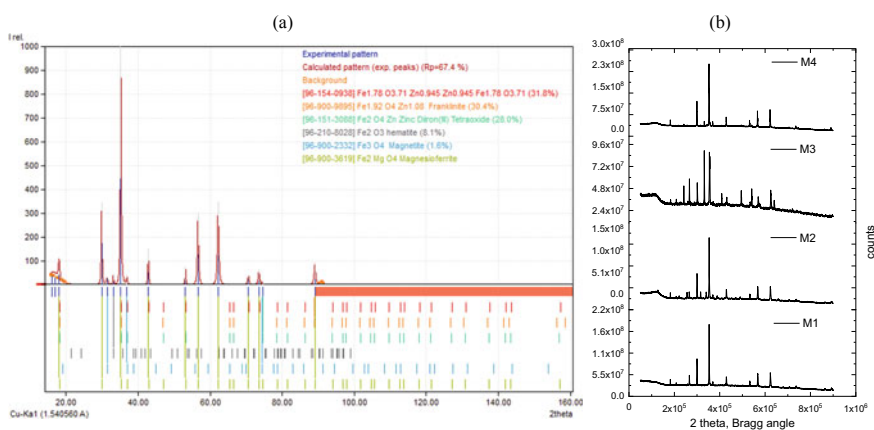
**Fig. 4** a XRD diffraction patterns of sample M4 and b the four samples simultaneously

Table 4 Main spinel phases shown in samples M1, M2, M3, and M4 identified and quantified by XRD

Samples	Fe ₂ O ₃	Fe _{2.96} O ₄	Fe ₃ O ₄	ZnFe ₂ O ₄	Zn _{0.54} Fe _{2.46} O ₄	Zn _{0.97} Fe _{2.02} O ₄	Zn _{1.08} Fe _{1.92} O ₄	Zn _{0.95} Fe _{1.78} O _{3.71}	Zn ₂ (SiO ₄)
M1			64.70		35.30				
M2		20.70	61.80	2.10					15.50
M3	8.00		7.40	73.20		11.40			
M4	8.10		1.70	28.00			30.40	31.80	

Table 5 Main spinel phases shown in samples M'1, M'2, M'3, and M'4 identified and quantified by XRD

Samples	Quartz low	Fe ₃ O ₄	ZnFe ₂ O ₄	SiO ₂ -coesita	Fe ₂ O ₃	Zn ₂ (SiO ₄)	Rwp	gof
	Icsd 16331	Icsd 85806	Icsd 91827	Icsd 18112	Icsd 82902	Icsd 20093		
M'1	6.00	10.10	64.20	1.70	18.00		4.14	1.23
M'2	5.60	24.20	51.10	1.40		17.7	4.72	1.44
M'3	5.60	21.60	71.10	1.70			4.42	1.40
M'4	6.40	3.70	36.40	1.70	51.80		4.35	1.30

(2.10%) as non-stoichiometric or mixed spinels: 31.80% Zn_{0.95}Fe_{1.78}O_{3.71} (M4); 30.40% Zn_{1.08}Fe_{1.92}O₄ (M4); Zn_{0.97}Fe_{2.02}O₄ (M3); and 35.30% Zn_{0.54}Fe_{2.46}O₄ (M1). Samples M3 and M4 observed a total of 84.60 and 90.20% of spinel phases, respectively. The interesting thing is that other magnetic phases were also observed such as: hematite Fe₂O₃, non-stoichiometric magnetite Fe_{2.96}O₄, stoichiometric magnetite Fe₃O₄. However, only in the case of M3 and M4 the hematite content is very similar. While samples M'1, M'2, M'3, and M'4 did not show the presence of non-stoichiometric zinc ferrites or spinel phases and a lot of SiO₂ contamination, possibly due to the excessive blow of the pistil on a porcelain crucible during the 48 h of grinding. It is notable that the fit between the experimental diffractograms and those adjusted by the Rietveld “gof” (Goodness of Fit) method of all tests are quite close to one (1).

Magnetic Characterization—VSM

The estimation results of the saturation magnetization (M) using Vibrating Sample Magnetometer—VSM or as a function of the applied magnetic field (H) carried out on the samples M1, M2, M3, M4, and M5, are shown in Table 6.

From Table 6, the highest saturation magnetization (M) observed, M5, was 0.68 emu/g, a value much lower than that observed for nanoparticles synthesized by green methods (12.81 emu/g) [10]. In Fig. 5a, the clearly marked magnetization

Table 6 Saturation magnetization (M) results of samples M1, M2, M3, M4, and M5

Muestras	Magnetización de saturación (emu/g)	Masa (g)
M1	0.20	0.04
M2	0.15	0.08
M3	0.15	0.05
M4	0.20	0.02
M5	0.68	0.09

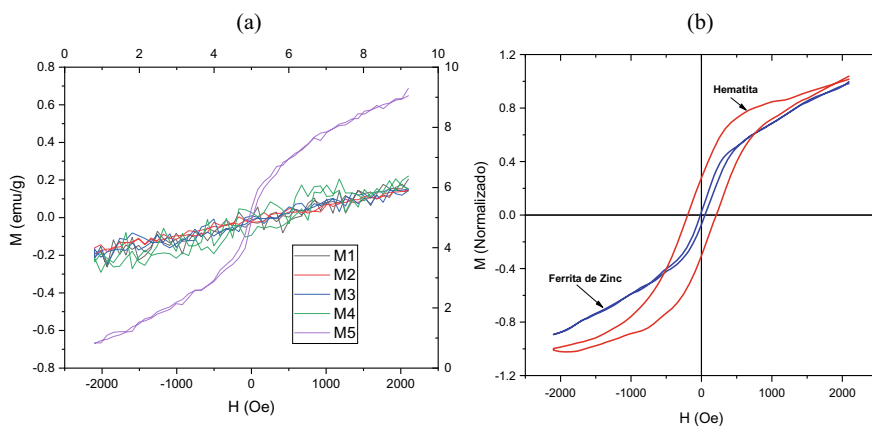


Fig. 5 Magnetization (M) as a function of the applied magnetic field (H) for samples M1, M2, M3, M4, and M5, and **b** normalized hysteresis curve as a function of the applied magnetic field of the equimolar zinc ferrite (M5) and hematite

hysteresis curve could only be observed in sample M5 because it is the standard sample M5. In Fig. 5b, the hysteresis of the sample of pure hematite (HM) and zinc ferrite (ZF) can be observed.

As can be seen in Fig. 5b, the magnetization observed in this zinc ferrite sample with spinel structure is due to the contribution of Fe^{2+} cations. As is known, these ions tend to occupy the tetrahedral gaps or interstices as occurs in normal spinel, thus forcing some Fe^{3+} to leave their tetrahedral positions towards the octahedral sites, but when it is the case of the occurrence of inverse spinels, these cations aligned and contribute to increasing the magnetization of the material, as it is the case with sample M5, but not with samples M1, M2, M3, and M4. A very weak paramagnetic behavior was observed in the magnetic characterization of M1, M2, M3, and M4 except in the case of M5 which is slightly magnetic.

Optical Characterization-UV Vis

Figure 6 shows both the (a) absorbance and (b) reflectance as a function of wavelength, in the range of 300 and 700 nm, of the four samples under study (M1, M2, M3, and M4).

In Fig. 6a, it is clearly observed that both samples M1 and M2 have almost the same behavior regarding the absorbance of the electrons emitted by the spectrophotometer, only sample M3 absorbed more energy than sample M4 and this, at its time, adsorbed more photon energy than M1 and M2 from the electron beam in a range between 450 and 700 nm while Fig. 6b shows the reflectance as a function of wavelength, in the range of 300 and 700 nm, for samples M1, M2, M3, and M4.

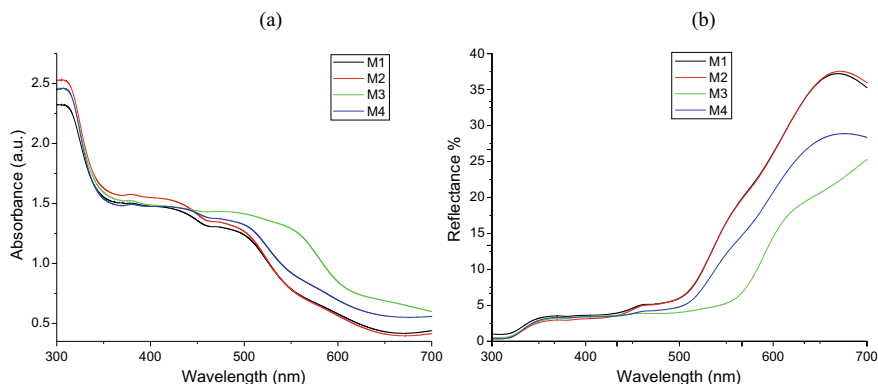


Fig. 6 **a** Absorbance and **b** reflectance spectra of samples M1, M2, M3, and M4 as a function of wavelength

Analogously to the previous case, it is observed that both samples M1 and M2 have almost the same behavior regarding the reflectance of the electrons emitted by the spectrophotometer, in turn, these showed a higher % of reflectance, compared to sample M4 and this consequently with sample M3 in the visible spectrum range between 450 and 700 nm.

From the results in Fig. 6 and using a spreadsheet to make the fundamental adjustments of the Kubelka–Munk function, the bandgap energies (E_g) of samples M1, M2, M3, and M4 could be estimated. Figure 7a shows the graph of the modified Kubelka–Munk function as a function of the photon energy in eV, of the four samples under study (M1, M2, M3, and M4) and Fig. 7b a summary of the magnetic and optical properties of samples M1, M2, M3, and M4.

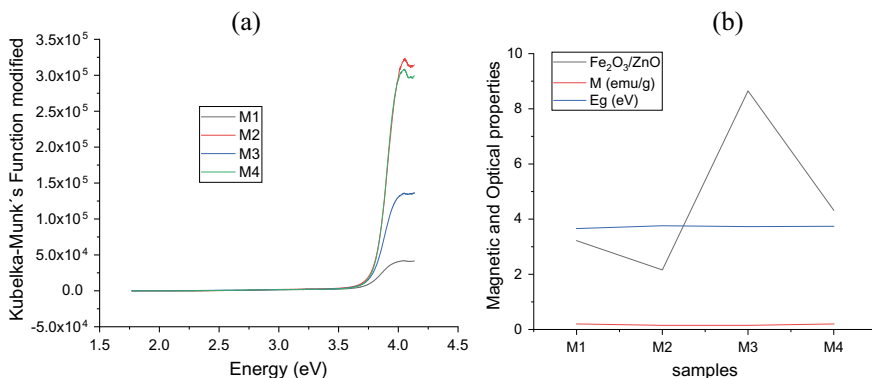


Fig. 7 **a** Estimation of the Kubelka–Munk Function as a function of the photon energy and **b** a summary of the magnetic and optical properties of samples M1, M2, M3, and M4 as a function of the Fe_2O_3 / “ratio” ZnO

Table 7 Bandgap energy values (E_g) of samples M1, M2, M3, and M4

Samples	E_g (eV)	Type of material	E_g (eV)
M1	3.66	Conductors	0.0
M2	3.76	Semiconductors	0.5–4.0
M3	3.73	Insulators	5.0–10.0
M4	3.74		

The UV–visible spectral analysis revealed interesting optical properties of samples M1, M2, M3, and M4: absorbance and reflectance, and above all it was possible to estimate an almost constant bandgap range (E_g), which indicates that these samples have a large amount of photon energy possible, classifying as “moderately semiconducting” according to the classification tables already widely disseminated (See Table 7).

UV–visible reflectance spectrometry analyses showed a bandgap variation of the samples M1, M2, M3, and M4 that presented values between 3.66 and 3.76 eV that are very high compared to other zinc ferrite nanoparticles produced using the green synthesis method via honey-mediated sol–gel combustion method [8]. UV–visible spectral analysis revealed optical properties and therefore the optical bandgap could be found using the Kubelka–Munk function diagram [9]. Photoluminescence studies exhibited the excitation wavelength, which showed a recombination of holes and electrons [10].

Conclusions

The large number of peaks or temperatures of probable decomposition, rearrangement or nucleation of new grains of zinc ferrites within the samples tested by TGA: S1, S2, S3, and S4 are due to the variety of spinel phases observed and quantified via XRD in samples M1, M2, M3, and M4. The weight loss observed via DTG was minimal. XRD of samples M1, M2, M3, and M4 showed the presence of the main inverse spinel phases, both the stoichiometric: $ZnFe_2O_4$ in M3 (73.20%), M4 (28.00%), and M2 (2.10%) and the non-stoichiometric or mixed spinels: 31.80% $Zn_{0.95}Fe_{1.78}O_{3.71}$ (M4); 30.40% $Zn_{1.08}Fe_{1.92}O_4$ (M4); $Zn_{0.97}Fe_{2.02}O_4$ (M3); and 35.30% $Zn_{0.54}Fe_{2.46}O_4$ (M1). Samples M3 and M4 observed a total of 84.60 and 90.20% of spinel phases, respectively. Other magnetic phases such as: hematite Fe_2O_3 , non-stoichiometric magnetite $Fe_{2.96}O_4$, stoichiometric magnetite Fe_3O_4 were also observed. However, only in the case of M3 and M4 the hematite content is very similar. Additionally, samples M'1, M'2, M'3, and M'4 did not exhibit non-stoichiometric zinc ferrites or spinel phases, but they did exhibit a lot of SiO_2 contamination, possibly due to the excessive blow of the pistil on the porcelain crucible during the 48 h of grinding. It is notable that the fit between the experimental diffractograms and those adjusted by the Rietveld “gof” (Goodness of Fit) method of all tests are quite close to one (1). On the other hand, samples M1, M2, M3,

and M4 observed a weakly paramagnetic behavior against the saturation magnetization of the VMS (between 0.5 and 1.0 eum/g), except in the case of M5 (0.68 eum/g) which observed a well-established hysteresis curve. The estimation results of the bandgap energy (E_g) via the manipulation of the Kubelka–Munk theory (modified Kubelka–Munk function) allowed us to determine that samples M1, M2, M3, and M4 are considered semiconductors (3.66 and 3.76 eV).

Acknowledgements Authors would like to thank the Research Vice Rectorate and the College of Geological Mining and Metallurgical Engineering Research Institute of the National University of Engineering for the financial assistance granted, without which these programmed experiences could not have been carried out.

References

1. Sugi S, Radhika S, Padma CM (2022) Co-precipitation of zinc ferrite nanoparticles in the presence and absence of polyvinyl alcohol with other constant parameters and the analysis of polyvinyl alcohol mediated zinc ferrite nanoparticles. *Mater Chem Phys* 292:126799
2. Mouhib Y, Belaiche M, Elansary M, Ferdi CA (2022) Effect of heating temperature on structural and magnetic properties of zinc ferrite nanoparticles synthesized for the first time in presence of Moroccan reagents. *J Alloy Compd* 895:162634
3. Cobos MA, de la Presa P, Llorente I, García-Escorial A, Hernando A, Jiménez JA (2020) Effect of preparation methods on magnetic properties of stoichiometric zinc ferrite. *J Alloy Compd* 849:156353
4. Afkhami A, Sayari S, Moosavi R, Madrakian T (2015) Magnetic nickel zinc ferrite nanocomposite as an efficient adsorbent for the removal of organic dyes from aqueous solutions. *J Ind Eng Chem* 21:920–924
5. Gómez-Marroquín MC (2004) Contribution to the study of the formation and reduction of Zinc Ferrite. Thesis dissertation, Department of Science of the Materials and Metallurgy, Pontifical Catholic University of Rio de Janeiro. DCMM - PUC-Rio, 2004, 179 p. Adviser: Prof. D'Abreu, José Carlos
6. Naik MM, Naik HB, Nagaraju G, Vinuth M, Naika HR, Vinu K (2019) Green synthesis of zinc ferrite nanoparticles in Limonia acidissima juice: characterization and their application as photocatalytic and antibacterial activities. *Microchem J* 146:1227–1235
7. Singh NB, Agarwal A (2018) Preparation, characterization, properties and applications of nano zinc ferrite. *Mater Today Proc* 5(3):9148–9155
8. Yadav RS, Kuřitka I, Vilcakova J, Urbánek P, Machovsky M, Masař M, Holek M (2017) Structural, magnetic, optical, dielectric, electrical and modulus spectroscopic characteristics of $ZnFe_2O_4$ spinel ferrite nanoparticles synthesized via honey-mediated sol-gel combustion method. *J Phys Chem Solids* 110:87–99
9. Kombaiiah K, Vijaya JJ, Kennedy LJ, Bououdina M, Al-Lohedan HA, Ramalingam RJ (2017) Studies on *Opuntia dillenii* haw mediated multifunctional $ZnFe_2O_4$ nanoparticles: optical, magnetic and catalytic applications. *Mater Chem Phys* 194:153–164
10. Vinosha PA, Mely LA, Jeronsia JE, Krishnan S, Das SJ (2017) Synthesis and properties of spinel $ZnFe_2O_4$ nanoparticles by facile co-precipitation route. *Optik* 134:99–108